Activated Stromal Cells Transfer Mitochondria to Rescue Acute Lymphoblastic Leukaemia Cells from Oxidative Stress.

Richard Burt[1], Aditi Dey[1], Sarah Aref[1], Melanie Aguiar[1], Ayse Akarca[1], Katharine Bailey[1], William Day[1], Steven Hooper[2], Amy Kirkwood[4], Kristina Kirschner[5], Soo-Wah Lee[1], Cristina Lo Celso[2,3], Jiten Manji[1], Marc R. Mansour[1], Teresa Marafioti[1], Rachel J. Mitchell[1], Robert C. Muirhead[1], Kenton Cheuk Yan Ng[1], Constandina Pospori[2,3], Ignazio Puccio[1], Krisztina Zuborne-Alapi[1], Erik Sahai[2] and Adele K. Fielding[1*]

1. UCL Cancer Institute, 72 Huntley St London WC1E 6DD

2. The Sir Francis Crick Institute, 1 Midland Road London NW1 1AT

3. Imperial College London, Sir Alexander Fleming Building, South Kensington Campus, London SW7 2AZ

4. CRUK and UCL Cancer Trial Centre, 90 Tottenham Court Road, London, WC1

5. Institute for Cancer Sciences, University of Glasgow, Glasgow, G61 1BD, UK

* to whom correspondence should be addressed at a.fielding@ucl.ac.uk

Running head: MSC transfer mitochondria to protect ALL cells

Text 3999 words **Abstract** 235 words, **Figures** 7, **Tables** 1, **References** 29

Scientific category: Lymphoid neoplasia

Key points

BM-derived MSC can become cancer associated fibroblasts and transfer mitochondria to rescue B-ALL cells from ROS-inducing chemotherapy.

Rescue of B-ALL cells is overcome by microtubule inhibitors which interrupt the tunnelling nanotubes used for mitochondrial transfer.

Abstract

We investigated and modelled the mesenchymal stromal cell (MSC) niche in adult acute lymphoblastic leukaemia (ALL). We used gene expression profiling, cytokine/chemokine quantification, flow cytometry and a variety of imaging techniques to show that MSC directly isolated from the primary bone marrow specimens of patients with ALL frequently adopted an activated, cancer-associated fibroblast phenotype. Normal, primary human MSC and the MSC cell line HS27a both became activated *de novo,* when exposed to the reactive oxygen species (ROS)-inducing chemotherapy agents cytarabine (AraC) and daunorubicin (DNR), a phenomenon blocked by the anti-oxidant N-acetyl cysteine. Chemotherapy-activated HS27a cells were functionally evaluated in a co-culture model with ALL targets. Activated MSC prevented therapy-induced apoptosis and death in ALL targets, via mitochondrial transfer through tunnelling nanotubes (TNT). Reduction of mitochondrial transfer by selective mitochondrial depletion or interference with TNT formation by microtubule inhibitors such as vincristine (VCR) - prevented the 'rescue' function of the activated MSC. Corticosteroids – also a mainstay of ALL therapy – prevented the activation of MSC. We also demonstrated that AraC (but not VCR) - induced activation of MSC, mitochondrial transfer and mitochondrial mass increase in a murine NSG model of disseminated SEM-derived ALL wherein CD19+ cells closely associated with nestin+ MSC after AraC but not the other conditions. Our data propose a readily clinically-exploitable mechanism for improving treatment ALL in which traditional, ROS-inducing chemotherapies are often ineffective at eradicating residual ALL, despite efficiently killing the bulk population.

Introduction

Relapse in ALL arises from putatively dormant, tumour-initiating cells which contribute to minimal residual disease (MRD), typically quantified by PCR-amplification of patient-specific immunoglobulin heavy chain/T cell receptor (Ig/TCR) gene re-arrangements[1]. MRD monitoring shows that relapsed ALL usually has the same Ig/TCR re-arrangements found at diagnosis. The intra-clonal origins of relapsed ALL are typically accepted [2]. Murine models also suggest that relapse of ALL does not necessarily arise from genetically-distinct, chemo-resistant cells, but more likely occurs due to protection of a subset of cells within a specific niche[3,4]. The niche identified by Duan *et al*[3] was induced by cytarabine (AraC, a DNA synthesis inhibitor) and daunorubicin (DNR, which intercalates DNA and prevents topoisomerase II progression) and was composed of homogeneous mesenchymal stromal cells (MSC) expressing nestin and α–smooth muscle actin (αSMA). By contrast, recent data in a T-ALL model in which corticosteroids and vincristine (VCR) were used as therapy suggested that T-ALL cells may have a more dynamic interaction with bone marrow, without a specific niche[5]. An important difference between the 'niche' and 'no niche' findings is the chemotherapy agents used to generate the model. 'Niche-generating' AraC and DNR are DNA damaging agents which trigger reactive oxygen species (ROS) in target cells and contrast with corticosteroids (potent anti-inflammatory agents) and VCR (a microtubule inhibitor) in mechanism of action. The reasoning that ROS generation could be critical to niche formation is consistent with a recent study of patient-derived xenograft models of acute myeloid leukaemia (AML) in which cells that were resistant to AraC showed very high ROS and increased mitochondrial mass. This suggested to us that

chemotherapy-induced ROS perturbation might correlate with ALL chemosensitivity within the niche [6].

To investigate, we sought evidence for a protective MSC niche using primary specimens from 70 patients enrolled in UKALL14 trial (NCT 01085617). We noted the frequent presence of activated MSC/cancer associated fibroblasts (CAF), a phenomenon hitherto not described in ALL. We further modelled this process *de novo*, with *in vitro* work using both primary MSC from healthy donors and an MSC cell line, HS27a as well as an *in vivo* model of ALL. CAF/activated MSC could prevent ALL cell apoptosis and death from exogenously-administered ROS-inducing agents by mitochondrial transfer along tunnelling nanotubes. Corticosteroids prevented the activation of CAF and VCR prevented the formation of the intracellular connections necessary for their ability to 'rescue' ALL cells from chemotherapy.

Methods

Cells

Human specimens and consent

All primary material was used with informed consent in accordance with the Declaration of Helsinki. (16/LO/2055)

Primary MSC Isolation and Expansion

Mononuclear cells (MNC) were isolated by density gradient centrifugation (Ficoll, Amersham Biosciences, Bucks, UK). MSC were isolated and expanded in Mesencult plus Mesencult stimulatory supplements (STEMCELL^{TM} Technologies) plus, 100

units/ml penicillin G, 100mg/ml streptomycin, 2mM L-glutamine (PenStrepGlut) (Gibco) and 1ng/ml basic FGF (R&D Systems). Passage 4-5 MSC were used in experiments. Cell supernatants used were from passage 1 or 2. MSCs were characterized based on the International Society for Cellular Therapy (ISCT)[7] criteria, using the Human MSC Functional Identification (R&D Systems) and Human MSC Verification kits, (R&D Systems).

Cell Lines

Human MSC cell line HS27a (ATCC), B-precursor ALL cell lines REH[8], SD1[9], SEM[10], TOM1[11] and murine MSC MS5 (all DSMZ) were grown in RPMI 1640 (MS5, αMEM) with 5-20% FBS and Pen-Strep-Glut.

MSC and ALL co-culture

MSC were plated on Day 0, ALL cells were added at 24 hours at 1:4 ratio. The cells were flow-sorted for use after 3-5 days. For transwell experiments, the ALL cells were added onto a transwell insert (0.4 - 1.0 μm) (Greiner Bio-one) at Day 1.

Mitochondrial depletion

HS27a cells were cultured in media containing 0.1μg/ml ethidium bromide, 50 μg/ml uridine and 1mM sodium pyruvate for 4 weeks.

Immunocytochemistry

Cells were fixed with 4% paraformaldehyde, washed, blocked for 2 hours with 1% bovine serum albumin (BSA), 10% normal donkey serum (Abcam) and 0.3% Triton X-100 (Sigma Aldrich). Primary antibody and antibodies were added for one hour each. DAPI (Santa Cruz Biotechnology) and F-actin stain Phalloidin-Atto 633 (Sigma

Aldrich) stain were added for 10 minutes. Images were acquired on the Zeiss axio-observer Z1 at room temperature with objectives 10xair Plan-NEOFLUAR NA 0.3, 20xair Plan-NEOFLUAR NA 0.4 and 40xair Plan-NEOFLUAR NA 0.75 using Axiovision Rel. 4.8 software and AxioCam MR Rev 3 camera. Fluorochromes used include DAPI, red fluorescent protein and cyanine5. No image adjustments were required.

Flow Cytometry

Samples were incubated with relevant antibodies at 4°C for 30 minutes. Fluorescence-minus-one controls were used to account for non-specific background staining. Ten thousand intact single cell events were collected on a BD LSRFortessa X-20 (Becton Dickinson, Oxford, UK). MSC were sorted from ALL cells antiCD90-FITC and antiCD19-APC on BD FACSARIA Fusion. Data analysis was with FlowJo software (version 10.4.2).

Mitochondrial transfer

MSC were stained with MitoTracker™ Deep Red (ThermoFisher M22426) according to manufacturer's instruction at 37°C for 30 mins. The cells were washed twice, then left for three hours to eliminate unbound probe prior to a final wash. The stained MSC were co-cultured with ALL cells for 24 – 72 hours. Mitochondrial transfer was quantified among the CD19-expressing ALL population.

Confocal time lapse imaging

Differentially stained cells were cultured on a 35mm glass bottom dish (Maktek) coated with 20µg/ml fibronectin at 37ºC on a heated tray at 5% CO_2. Chemotherapy was added immediately prior to imaging. Images were acquired on a Zeiss LSM 880

with Airyscan with objective 63xOil Plan-apochromat NA 1.40 at a resolution of 1024 x 1024 pixels in the *x* and *y* directions and 0.5µm steps in z direction. The pinhole diameter was set at 1 airy unit. DiO and Deep Red Mitotracker were excited with the 488 and 633 lasers respectively. Transmitted Photomultiplier Tube was used in transmitted mode to generate an image. Imaging processing was done with Oxford Instruments, BITPLANE Imaris 9.1 and Carl Zeiss ZEN Black.

Cell viability and apoptosis assay

MSC were co-cultured with ALL cells in a 6-well plate +/- AraC 200nM, DEX 200 – 1000nM, VCR 1.6nM. Other agents used were latrunculin-B 500nM, nocodazole 10-100nM, colchicine 1.6nM. At 48hrs the cells were collected and stained with CD19 before staining with Annexin V according to manufacturer's instruction, finally followed by DAPI. The CD19+ as analysed by flow for Annexin V/DAPI to determine apoptotic and dead cell populations.

ROS Quantification

MSC co-cultured with ALL cells in a 6-well plate with or without drugs. CellRox® Green (ThermoFisher C10444) staining was carried out at 24 hours, according to manufacturer's instruction and quantified by flow cytometry.

Quantification of secreted proteins

Cytometric Bead Array

Cytometric Bead Array (BD Biosciences) was carried out according to manufacturer's instruction using human IL6 Flex Set (BD Biosciences 558276), human IL-8 Flex Set (BD Biosciences 558277) or human MCP-1/CCL2

Flex Set (BD Biosciences 558287). Three hundred events/analyte from the live gate were collected on a BD FACSAria instrument (Becton Dickinson, Oxford, UK). Data were analysed using FCAP Array Software Version 3.0.

ELISA

Supernatant was collected from the MSCs at sub-confluence, passage 1-2 and stored at -80°C. Semi-quantitative 'screening' multi-analyte ELISAs were performed on the thawed, passage 1 cell supernatant, using custom-made kits (Custom Mix-n-Match Multi-Analyte ELISArray Kit, Qiagen 336111). Single analyte quantitative ELISA kits (supplementary methods table 2) were used on passage 2 supernatants.

MTS Tetrazolium cell viability assay

MTS (CellTitre 96®Aqueous One Solution Reagent) was done according to the manufacturer's instruction. Absorbance was read at 570nm on a BMG FLUOstar Galaxy absorbance reader.

RNA extraction

RNA was extracted from cells using TRIzol® (AMbion by Life Technologies, 15596026) and separated from DNA using chloroform (Sigma Aldrich). Isopropanol (Sigma Aldrich) was added and the samples were frozen at -80°C overnight. Following thawing and washing with 70% ethanol the pellet of RNA was re-suspended in RNase free water and the concentration measured on a NanoDrop.

RT^2 Profiler PCR Array

cDNA was synthesised using the RT2 first strand kit (Qiagen - 330401) according to manufacturer's instruction. The cDNA was then used for RT^2 Profiler PCR array

according to the manufacturer's protocol with a pre-defined and pre-prepared selection of primers for appropriate CAF defining targets listed in supplementary methods, table 3. Each sample was run in triplicate for each gene and quantified relative to GAPDH housekeeping control.

Mitochondrial DNA detection

DNA was extracted from cells using QIAamp® DNA Blood Mini Kit (Qiagen 51106). The DNA was amplified for detection of mitochondrial and nuclear DNA from both human and mouse using the primers below. Annealing temperature used was 60 degrees for 15 to 25 cycles. The PCR product was run in 2% agarose (SIGMA) gel and visualised under UV.

Mouse model

Disseminated BFP-luciferase-SEM leukaemia was established in 16 8-10-week-old NSG mice by tail vein injection. Mice were treated with AraC, VCR, nocodazole, AraC with VCR or PBS control. The experimental schema is shown in supplementary figures. At sacrifice, SEM cells were flow sorted and MSC were cultured and the assays shown were carried out as described. One femur per mouse was sent for histopathology. See supplementary methods for detail.

Statistical analysis

The data was analysed on GraphPad Prism 6 software except where indicated. For statistical comparisons Chi-squared, unpaired student t-tests or Mantel-Cox test were used, as indicated.

Results

To explore the stromal fibroblast niche in ALL, we isolated (68/84) and expanded (37/68) MSC from 84 B-ALL bone marrow specimens from 70 patients (table 1) participating in the UKALL14 trial. A significant difference in apparent CAF-related morphology between specimens taken after VCR and DEX exposure (6 of 16, 38%) and those taken after AraC-exposure (20 of 25, 80%, p=0.006) prompted a more comprehensive documentation of CAF, defined by pro-inflammatory cytokine secretion, altered morphology with prominent actin stress fibres and a typical gene expression profile (GEP). As shown in Figure 1, after combined VCR, dexamethasone (DEX) and DNR exposure, the IL8, CCL2, CXCL1, CXCL2 and IL6 secretion patterns appeared similar to those seen in the healthy donor MSC, contrasting with an increase after AraC-containing treatment. In figure 1b, Phalloidin and DAPI staining of three samples from each time-point, (red arrows in figure 1a, based on available material) shows prominent F-actin- stress fibres (indicated by red boxes around the images) at diagnosis and after AraC but not in healthy donors or after VCR/DEX. The same specimens in figure 1c showed strong upregulation of CAF-associated genes. The unexpected findings of CAF among primary patient ALL specimens prompted us to model their generation by chemotherapy drugs.

First, we evaluated whether clinically-relevant concentrations of DNR, AraC, VCR and DEX could generate CAF from healthy donor and/or HS27a MSC. Figure 2a shows typical CAF cytomorphology in both HS27a and normal healthy donor MSC after AraC and DNR but not DEX and VCR. GEP (figure 2b) shows that AraC and DNR generated similar CAF-like chemokine and cytokine gene upregulation seen in patient specimens, with MMP-1 upregulation particularly prominent. VCR upregulated chemokine and cytokine gene expression modestly, but not cytoskeletal

and ECM remodelling and growth factor gene expression. After DEX, there was striking downregulation of MMP-1. The corresponding cytokine/chemokine levels (figure 2c) confirm the pro-inflammatory impact of AraC, DNR and VCR, by contrast to anti-inflammatory impact of DEX. To study the functional impact, we 'primed' HS27a by exposure to AraC, VCR or DEX (DNR was excluded as it, paradoxically, extended MSC lifespan), then quantified the survival of a co-cultured B-ALL cell line SEM (specifically chosen for its low intrinsic ROS levels and known AraC susceptibility) exposed to the same agents. As shown in figure Figure 2d (i-iii), a clear pattern of reduced response to AraC, DEX or VCR was seen when the MSC were primed with AraC (red arrows) but not with the other agents. A transwell set-up (figure 2d (iv)) abolished this impact.

Next, we tested the concept that control of oxidative stress, via modification of reactive oxygen species (ROS) could explain the chemotherapy-induced support provided by activated MSC to ALL cells. First, we showed in figure 3a panel (i), that AraC and DNR treatment of SEM ALL directly elevated ROS. VCR had no impact, whilst DEX reduced ROS. Figure 3a panel (ii) shows the functional impact in monoculture and co-culture; whilst all four drugs expectedly readily killed SEM cells, co-culture of SEM with HS27a MSC lowered AraC-driven cell death by two thirds, DNR-driven death by one third, VCR by about one half but DEX, not at all. To confirm the relationship of ROS to the chemotherapy-induced MSC activation, we performed reversibility experiments with N-acetyl cysteine (NAC), a glutathione precursor antioxidant. As shown in figure 3b, NAC alone did not impact HS27a cells whereas NAC prevented both AraC and DNR-induced activation. To confirm the critical functional role of ROS control by activated MSC, we quantified ROS, apoptosis and cell death of SEM ALL cells after AraC therapy, either alone or in co-

culture with HS27a MSC. Figure 3c(i) shows that whilst AraC significantly increased ROS in SEM cells in monoculture, ROS levels were significantly lowered in co-culture with HS27a and were no longer impacted by AraC. The corresponding panels ii and iii show that the MSC-mediated control of ROS control significantly impacted AraC-mediated SEM cell apoptosis and cell death. Cell-cell contact was critical – the 'chemoprotection' of SEM by HS27a was completely lost without direct contact (figure 3d). To further confirm the relevance of ROS, figure 3e shows that NAC significantly reduced AraC-induced ROS and apoptosis. A reduction in cell death was also apparent, albeit not reaching statistical significance.

Next, we investigated the mechanism for the ROS-induced, MSC-mediated chemoprotection of ALL cells. As shown in figure 4a, images of healthy donor and SEM co-cultures taken after therapy with AraC show close contact. By contrast, after treatment with VCR, contact between the co-cultured cells was minimal. Based on published evidence of mitochondrial transfer between MSC and ALL cells[12], we hypothesised that mitochondrial transfer between activated MSC and B-ALL cells, via tunnelling nanotubes (TNT), could explain the CAF-mediated protection of ALL cells from ROS-inducing chemotherapy. First, we used a MitoTracker ^{TM} assay in which a fluorescent dye irreversibly labels mitochondria, to quantitate mitochondrial transfer. Figure 4b(i) shows that mitochondrial transfer to B-ALL cells occurred after HS27a cells, stained prior with MitoTracker ^{TM}, were co-cultured with 3 different B-ALL cell lines (SD1, TOM-1 and SEM). This was in proportion to baseline ROS (data not shown). Cell-cell contact was obligatory – mitochondrial transfer was abolished by transwell. Similarly, Figure 4b(ii) shows that spontaneous mitochondrial transfer to three primary ALL specimens - but not primary B cells - occurred after co-culture with MitoTracker ^{TM} -stained healthy donor MSC. Figure 4c (i) shows that AraC, but not

VCR or DEX, stimulated the mitochondrial transfer to SEM ALL cells. In figure 4d we confirmed that NAC significantly abrogated both AraC and DNR-stimulated mitochondrial transfer to both SEM and REH ALL cells. Next, we directly visualised the transfer of mitochondria along tunnelling nanotubes by time-lapse confocal imaging. The arrows in figure 4e indicate the progress of two individual mitochondria over approximately 20 minutes. Finally, to exclude any possibility of passive transfer of mitochondria, we used the murine stromal line MS5 as an alternative mitochondria donor. In figure 4f, murine mitochondrial, but not nuclear, DNA is clearly seen in flow-sorted SEM cells after co-culture, both at baseline and at higher levels after AraC treatment. Taken together, our data clearly suggested a role for mitochondrial transfer from activated MSC to ALL cells, in protection against ROS.

To further confirm the functional relevance of mitochondrial transfer, we studied the extent to which inhibition of mitochondrial transfer impacted the ability of MSC-CAF to protect ALL cells. First, we generated HS27a cells deficient in mitochondria following prolonged culture with low dose ethidium bromide and uridine which selectively depletes mitochondrial DNA[13,14]. Depletion was confirmed as shown in Figure 5a panels (i) and (ii), by PCR for mitochondrial DNA and mitotracker® imaging in depleted cells and non-depleted controls. The mitochondria-depleted HS27a retained viability, became activated and retained capability to interact with SEM cells as imaged in figure 5a (iii). However, the mitochondria-depleted HS27a cells were clearly defective in their ability to rescue SEM ALL cells from AraC-induced apoptosis (figure 5a(iv)) and cell death (figure 5a(v)). Next, we used various microtubule inhibitors to block mitochondrial transfer. Figure 5b shows that both the actin polymerisation inhibitor latrunculin-B and the microtubule inhibitor, nocodazole, significantly blocked AraC-stimulated mitochondrial transfer from HS27a

to ALL cells. Then, we quantified the impact of blocking mitochondrial transfer on AraC-mediated SEM cell killing using the HS27a/SEM co-culture system. First, we confirmed (Fig 5c(i and ii)) that none of the agents used were directly toxic to HS27a or SEM cells in monoculture with the exception of VCR and SEM. In figure 5b (ii) we show that in the HS27a/SEM co-culture, latrunculin-B, nocodazole and colchicine all partially, but significantly, ablated HS27a MSC-mediated protection from AraC. VCR entirely ablated the protection, completely restoring AraC toxicity with superadded SEM cell killing, due to its own cytotoxic properties. Figure 5c(iii) shows that the morphological changes seen in activated HS27a cells are altered by nocodazole and colchicine by a clear diminution of visible connections between cells despite the lack of impact on HS27a viability.

Due to the clinical importance of combination therapy in the treatment of ALL, we confirmed that combining AraC or DNR with VCR or DEX could block key aspects of MSC activation. In figure 6a, both AraC and DNR activate HS27a MSC but when either drug is used together with either VCR or DEX, the morphological hallmarks of activation do not occur, nor (figure 6b) the typical CAF cytokine secretion profile. ~~DEX appears to prevent activation to CAF and VCR acts to prevent the consequences.~~

To demonstrate *in vivo* relevance, we generated a disseminated model of ALL by tail vein injection of 2 x 10^6 blue fluorescent protein/luciferase-labelled SEM cells. The experimental schema is shown in supplementary figure S1. Three days after confirmed engraftment mice were treated with either PBS control, AraC, VCR or nocodazole then sacrificed three days later. All agents except PBS control rapidly reduced the leukaemia burden (figure 7a i and ii). MSC isolated and cultured from the murine bone marrow after AraC showed the typical appearance of CAF by

phalloidin, DAPI and αSMA expression which was not evident in control-treated mice (figure 7b i and ii). As shown in figure 7c, both ROS levels (7ci) and mitochondrial mass (7cii) were significantly elevated in SEM cells after AraC, but not control, VCR or nocodazole-treatment of the mice. The presence of murine mitochondrial but not nuclear DNA in AraC-treated, sorted SEM cells is shown in supplementary figure S2. Figure 7d shows CD19 (brown) and nestin (pink) staining of sections of femur. Red boxes highlight CD19 ALL cells closely associated with nestin-stained niche in the AraC but not VCR condition. The complete histopathology set is shown in supplementary figure S3. In a therapeutic experiment, five mice/group were treated to humane endpoint with PBS, AraC, VCR or AraC+VCR. Figure 7e (ii) shows that only the AraC+VCR combination improved survival compared to PBS control. In a separate cohort, where mice were sacrificed three days after treatment, mitochondrial mass had increased in the SEM cells only in response to AraC but not VCR and was at an intermediate level after AraC+VCR combination (Figure 7e (ii). In summary, we identified and cultured CAF directly from the bone marrow of patients with ALL undergoing chemotherapy. We modelled the activation process, which could be blocked by antioxidants, *in vitro* and *in vivo* by administration of ROS-inducing chemotherapy drugs. Transfer of mitochondria from CAF, along tunnelling nanotubes, prevented cell death from ROS-inducing chemotherapy in ALL cells. This cytoprotective process was interrupted, *in vitro* and *in vivo,* by agents that disrupt microtubule formation.

Discussion

We show that MSC isolated from the primary bone marrow of patients being treated for ALL commonly adopt an activated, cancer-associated fibroblast-like phenotype with cytoskeletal and gene expression changes and high-level proinflammatory cytokine secretion. The primary patient data are intriguing but predominantly hypothesis-generating, being limited by lack of access to longitudinal specimens. However, this does not detract from our frequent identification of CAF, the most abundant mesenchymal cell types present within most human carcinomas[15] but not previously shown in ALL. Among the key characteristics of the primary patient CAF were a 16-64-fold increase in transcription of MMP1, a 2-8-fold increase in transcription of Nbla00170 (nestin) and pro-inflammatory cytokine secretion, all consistent with descriptions of CAF in solid tumors [16].

To assess the mechanism of CAF generation of activated MSC and to understand their functional properties in supporting ALL targets[17], we used *in vitro* and *in vivo* niche models. We easily modelled CAF-formation from healthy donor or HS27a MSC *in vitro* using AraC and DNR at clinically-relevant concentrations. The *in vitro*, chemo-activated MSC appeared morphologically identical to the primary patient CAF with a very similar GEP and cytokine secretion pattern in our targeted panels. Activation clearly related to an AraC or DNR-mediated rise in intracellular ROS and was readily blocked by the antioxidant NAC. AraC-mediated increases in SEM target cell ROS levels were closely coupled to apoptosis and cell death in monoculture, but when co-cultured with MSC, target cell ROS levels, apoptosis and cell death was highly significantly abrogated. Cell-cell contact was clearly required

for the process of rescue from oxidative stress - rescue was absent when a transwell was used. An further dissection of the species ROS is important and is ongoing.

We uncovered mitochondrial transfer, through actin-containing, tunnelling nanotubes as the mechanism by which this MSC-mediated protection occurred. Whilst it is already known that ALL cells can use tunnelling nanotubes to communicate with MSC[12] and transfer of mitochondria between cell types is already a well-described phenomenon[18-22], the transfer of mitochondria in direct relationship to chemoprotection from ROS-inducing therapy, has not been described and is of particular and immediate relevance to the therapy of ALL. The four drugs we have used in our model are the mainstays of ALL treatment. Hyper CVAD[17], one of the most common therapeutic protocols used internationally for the treatment of ALL includes repeating blocks of relatively dose intensive AraC given without VCR or DEX. ~~Our data suggests that outcomes of such therapeutic combinations used in ALL might benefit from adjustment to ensure that microtubule damaging agents such as VCR or anti-inflammatory agents such as DEX are always given with ROS-inducing agents.~~ Our work demonstrates that when VCR or DEX are combined with AraC or daunorubicin, HS27a MSC do not develop the cytopathological hallmarks of activated MSC. All these findings – from the activation of MSC through to demonstration of mitochondrial transfer were recapitulated in a murine model.

Our data shed light on a prior study which showed that pre-leukaemic 'stem cells' cultured in a niche-like environment with MSC were uniformly sensitive to all microtubule damaging drugs or corticosteroids tested, in contrast to their resistance to the large majority of the other 1904 compounds tested [23]. The reason for those findings was not clear at the time, but our data suggest that support from the niche

provides an explanation. Our work is also consistent with evidence from solid organ malignancies [24,25] in which activation of stromal cells with cytotoxic chemotherapy induced a stromal cell state, characterised by enhanced ELR-motif cytokine secretion which aided cancer cell survival. Our data also give strong support to the use of stromal systems for drug discovery in ALL, as described by Frismantas *et al* [26]. Our data are also consistent with the findings of Ede et al in which MSC protected T-ALL from ROS-inducing parthenolide[27], albeit release of thiols was described as the mechanism. ~~It is likely that~~ Clearly, there are multiple mechanisms at play in these complex niches - of particular note is the association of human CD19+ cells with a nestin+ niche in the murine femora from AraC-treated mice. Mendez-Ferrer at al have previously shown that nestin^{+} MSC represent bona fide bone marrow niche with a close physical interaction with haematopoietic stem cells[28] and furthermore, that they can transfer mitochondria to AML cells[29].

In summary, our work couples previously disparate strands of evidence from the solid tumours with decades-old clinical observations in ALL, to develop a new, clinically-testable hypothesis on prevention of chemoresistance in ALL. We plan to directly test our observations in a proposed randomised clinical trial (UKALL15) comparing our current, standard-of-care regimen with a regimen wherein VCR and DEX are always given together with ROS-inducing agents such as AraC and DNR and appropriate, longitudinal specimens are collected to assess the relationship between MSC activation and outcome in clinical specimens.

Acknowledgements

RB was supported by the CRUK-UCL Centre Award/Clinical Training Award Cycle 2 [A20937] and a Lady Tata Memorial Trust International Award.

The UKALL14 trial was funded by grant to AKF CRUK/09/006 from CRUK.

The UKALL14 biobank was funded by grant C27995/A21019 to AKF and Anthony V. Moorman from CRUK.

We thank Bingli Liu for her contributions to this project.

Authorship contributions

RB performed experiments, designed experiments and wrote the paper. AD performed experiments and designed experiments. SA, AA, KB, MA, SH, SWL, TM, RJM, RM, KCYN, IP, CP and KZA performed experiments. WD advised and assisted with flow cytometry. AK supplied and analysed clinical data. KK advised on experimental design. JM advised and assisted with imaging. CLC designed and critically evaluated experiments. MRM critically evaluated experiments and provided supervision. ES designed and critically evaluated experiments and provided reagents. AKF conceived the project, obtained funding, designed and critically evaluated experiments, provided supervision and wrote the paper. All authors read and commented on the paper and approved the final version.

AKF would like to thank the 2018 European Haematology Association/American Society of Haematology Translational Research Training in Hematology Program faculty and students for helpful discussions.

The authors declare no conflicts of interest.

References

1. Bruggemann M, Schrauder A, Raff T, et al. Standardized MRD quantification in European ALL trials: proceedings of the Second International Symposium on MRD assessment in Kiel, Germany, 18-20 September 2008. *Leukemia : official journal of the Leukemia Society of America, Leukemia Research Fund, UK*. 2010;24(3):521-535.
2. van Delft FW, Horsley S, Colman S, et al. Clonal origins of relapse in ETV6-RUNX1 acute lymphoblastic leukemia. *Blood*. 2011;117(23):6247-6254.
3. Duan CW, Shi J, Chen J, et al. Leukemia propagating cells rebuild an evolving niche in response to therapy. *Cancer Cell*. 2014;25(6):778-793.
4. Ebinger S, Ozdemir EZ, Ziegenhain C, et al. Characterization of Rare, Dormant, and Therapy-Resistant Cells in Acute Lymphoblastic Leukemia. *Cancer Cell*. 2016;30(6):849-862.
5. Hawkins ED, Duarte D, Akinduro O, et al. T-cell acute leukaemia exhibits dynamic interactions with bone marrow microenvironments. *Nature*. 2016;538(7626):518-522.
6. Farge T, Saland E, de Toni F, et al. Chemotherapy-Resistant Human Acute Myeloid Leukemia Cells Are Not Enriched for Leukemic Stem Cells but Require Oxidative Metabolism. *Cancer Discov*. 2017;7(7):716-735.
7. Dominici M, Le Blanc K, Mueller I, et al. Minimal criteria for defining multipotent mesenchymal stromal cells. The International Society for Cellular Therapy position statement. *Cytotherapy*. 2006;8(4):315-317.
8. Greaves M, Janossy G. Patterns of gene expression and the cellular origins of human leukaemias. *Biochim Biophys Acta*. 1978;516(2):193-230.
9. Gora-Tybor J, Deininger MW, Goldman JM, Melo JV. The susceptibility of Philadelphia chromosome positive cells to FAS-mediated apoptosis is not linked to the tyrosine kinase activity of BCR-ABL. *Br J Haematol*. 1998;103(3):716-720.
10. Greil J, Gramatzki M, Burger R, et al. The acute lymphoblastic leukaemia cell line SEM with t(4;11) chromosomal rearrangement is biphenotypic and responsive to interleukin-7. *Br J Haematol*. 1994;86(2):275-283.
11. Okabe M, Matsushima S, Morioka M, et al. Establishment and characterization of a cell line, TOM-1, derived from a patient with Philadelphia chromosome-positive acute lymphocytic leukemia. *Blood*. 1987;69(4):990-998.
12. Polak R, de Rooij B, Pieters R, den Boer ML. B-cell precursor acute lymphoblastic leukemia cells use tunneling nanotubes to orchestrate their microenvironment. *Blood*. 2015;126(21):2404-2414.
13. Zylber E, Vesco C, Penman S. Selective inhibition of the synthesis of mitochondria-associated RNA by ethidium bromide. *J Mol Biol*. 1969;44(1):195-204.
14. Hayakawa T, Noda M, Yasuda K, et al. Ethidium bromide-induced inhibition of mitochondrial gene transcription suppresses glucose-stimulated insulin release in the mouse pancreatic beta-cell line betaHC9. *J Biol Chem*. 1998;273(32):20300-20307.
15. Mitchell MI, Engelbrecht AM. Metabolic hijacking: A survival strategy cancer cells exploit? *Crit Rev Oncol Hematol*. 2017;109:1-8.
16. Erez N, Truitt M, Olson P, Arron ST, Hanahan D. Cancer-Associated Fibroblasts Are Activated in Incipient Neoplasia to Orchestrate Tumor-Promoting Inflammation in an NF-kappaB-Dependent Manner. *Cancer Cell*. 2010;17(2):135-147.
17. Kantarjian HM, O'Brien S, Smith TL, et al. Results of treatment with hyper-CVAD, a dose-intensive regimen, in adult acute lymphocytic leukemia. *Journal of clinical oncology : official journal of the American Society of Clinical Oncology*. 2000;18(3):547-561.
18. Islam MN, Das SR, Emin MT, et al. Mitochondrial transfer from bone-marrow-derived stromal cells to pulmonary alveoli protects against acute lung injury. *Nat Med*. 2012;18(5):759-765.
19. Moschoi R, Imbert V, Nebout M, et al. Protective mitochondrial transfer from bone marrow stromal cells to acute myeloid leukemic cells during chemotherapy. *Blood*. 2016;128(2):253-264.

20. Marlein CR, Zaitseva L, Piddock RE, et al. NADPH oxidase-2 derived superoxide drives mitochondrial transfer from bone marrow stromal cells to leukemic blasts. *Blood*. 2017;130(14):1649-1660.
21. Jiang D, Gao F, Zhang Y, et al. Mitochondrial transfer of mesenchymal stem cells effectively protects corneal epithelial cells from mitochondrial damage. *Cell Death Dis*. 2016;7(11):e2467.
22. Shen J, Zhang JH, Xiao H, et al. Mitochondria are transported along microtubules in membrane nanotubes to rescue distressed cardiomyocytes from apoptosis. *Cell Death Dis*. 2018;9(2):81.
23. Gerby B, Veiga DF, Krosl J, et al. High-throughput screening in niche-based assay identifies compounds to target preleukemic stem cells. *J Clin Invest*. 2016;126(12):4569-4584.
24. Sun Y, Campisi J, Higano C, et al. Treatment-induced damage to the tumor microenvironment promotes prostate cancer therapy resistance through WNT16B. *Nat Med*. 2012;18(9):1359-1368.
25. Chan TS, Hsu CC, Pai VC, et al. Metronomic chemotherapy prevents therapy-induced stromal activation and induction of tumor-initiating cells. *J Exp Med*. 2016;213(13):2967-2988.
26. Frismantas V, Dobay MP, Rinaldi A, et al. Ex vivo drug response profiling detects recurrent sensitivity patterns in drug-resistant acute lymphoblastic leukemia. *Blood*. 2017;129(11):e26-e37.
27. Ede BC, Asmaro RR, Moppett JP, Diamanti P, Blair A. Investigating chemoresistance to improve sensitivity of childhood T-cell acute lymphoblastic leukemia to parthenolide. *Haematologica*. 2018;103(9):1493-1501.
28. Mendez-Ferrer S, Michurina TV, Ferraro F, et al. Mesenchymal and haematopoietic stem cells form a unique bone marrow niche. *Nature*. 2010;466(7308):829-834.
29. Forte D, García-Fernández M, Sánchez-Aguilera A, et al. Leukemic Stem Cells Co-Opt Normal Bone Marrow Niches As a Source of Energy and Antioxidant Defence. *Blood*. 2017;130(Suppl 1):94-94.

Table 1 Patient characteristics

Baseline Characteristic		MSC sample population	Not in MSC Sample	p-value*
		N=70	N=585	
Age, median (range)		43.0(22 - 65)	46.0(23 - 65)	0.068**
Sex				
	Male	48 (68.6)	310 (53.0)	0.013
	Female	22 (31.4)	275 (47.0)	
Baseline WBC, median (range)		11.0(.8 - 583.1)	7.9(.11 - 889.6)	0.24**
PH status				
	PH-	51 (73.9)	392 (68.7)	0.37
	PH+	18 (26.1)	179 (31.3)	
	Missing/failed	1	14	
T(4,11)				
	Absent	62 (91.2)	497 (92.4)	0.33
	Present	6 (8.8)	41 (7.6)	
	Missing/failed	2	47	
Complexity				
	Absent	53 (96.4)	425 (95.1)	0.97***
	Present	2 (3.6)	22 (4.9)	
	Missing/failed	15	138	
HoTr/Near-haploidy				
	Absent	55 (96.5)	409 (89.7)	0.10
	Present	2 (3.5)	47 (10.3)	
	Missing/failed	13	129	
Any Cytogenetic risk factors				
	Absent	28 (50.0)	186 (39.6)	0.13
	Present	28 (50.0)	284 (60.4)	
	Missing/failed	14	115	
High risk baseline				
	Standard risk	13 (19.4)	64 (11.5)	0.064
	High risk	54 (80.6)	492 (88.5)	
	Unknown,	13 (19.4)	64 (11.5)	0.064

*Chi-squared unless otherwise stated

**Wilcoxon Mann Whitney test

***Fisher's exact test

Figure legends

Figure 1 Activated fibroblasts are common in primary samples from patients with *de novo* ALL undergoing induction chemotherapy.

A. Cytokines and chemokines secreted by MSC isolated from the normal healthy donor bone marrow or primary patient ALL specimens at diagnosis and after first and second course of chemotherapy. IL8 (blue), CCL2 (red), CXCL1 (green), CXCL2 (purple), IL6 (orange), all in pg/ml are shown on the Y axis. X axis shows each sample denoted by UKALL14 trial number (UPN) or healthy donor number (HDN), Arrows below the X axis indicate the specimens which were subsequently evaluated in more detail

B. Photomicrographs (40X magnification), showing phalloidin and DAPI staining of MSC isolated from primary patient ALL indicated by UPN or HDN

C. Gene expression profile of showing fold upregulation (Y axis) of 18 selected genes in patient specimens - UPN indicated above the panel - at diagnosis and after first and second course of chemotherapy - compared to mean baseline of 3 normal healthy donors MSC - isolated from primary patient ALL. Red box around UPN indicates specimen with morphological changes. Gene names are shown on the X axis. A blue line is drawn at, 2-fold upregulation considered significant.

Figure 2 AraC and DNR activate MSC, *de novo* which abrogates B-ALL target cell responses to chemotherapy agents in co-culture .

A. Phalloidin, DAPI or αSMA staining (40x) of HS27a cells or healthy donor MSC: baseline or after exposure to the chemotherapy agents indicated.

B. Gene expression panel showing fold upregulation (compared to untreated) in HS27a cells after exposure to the chemotherapy agents indicated in (i) to (iv).

C. Cytokine bead assays for IL6 (i), IL8 (ii) and CCL2 (iii) (pg/ml, Y axis) following exposure of HS27a to the chemotherapy agents indicated on the X axis. All statistically significant comparisons (by unpaired t-test) are as depicted: IL8, none versus AraC, $P < 0.0001$, IL8, none vs. DNR, $P= 0.002$, IL8, none vs. DEX, $P= 0.001$, IL8, none vs. VCR, $P < 0.0001$. CCL2 none vs. AraC, $P= 0.0169$, CCL2, none versus DEX, $P = 0.0166$, CCL2, none vs. VCR, $P= 0.0065$

D. MTS assays showing relative viability of SEM cells (Y axis) after treatment with (i) AraC (ii) DEX (iii) VCR for 48 hours, after co-culture with HS27a cells previously 'primed' by chemotherapy pre-treatment denoted on the X axis. Data are shown relative to unprimed HS27a, set at 1. AraC primed HS27a are highlighted throughout with a red arrow. All statistically significant comparisons (by unpaired t-test) are as depicted: (i) no pre-treatment vs. VCR, $P = 0.041$, AraC vs. VCR, $P = 0.022$. (ii) no pre-treatment vs. VCR, $P = 0.0087$, AraC vs. VCR, $P = 0.0087$. (iii) no pre-treatment vs. VCR, $P = 0.0006$, AraC vs. VCR, $P = 0.0017$ (iv) MTS assay showing relative viability of SEM cells (Y axis) after transwell-culture with primed HS27a cells as denoted on the X axis. Data are relative to unprimed HS27a, set at 1. There are no statistically significant differences. All data are mean +/- SE of 3 independent experiments

Figure 3 Reactive oxygen species promote CAF formation and promote MSC-mediated chemoprotection

A. (i) ROS levels relative to untreated SEM baseline (1.0), Y axis, after exposure to chemotherapy agents indicated on the X axis (ii) percentage cell death (DAPI+, Y axis) of SEM cells exposed to the chemotherapy agents indicated either in monoculture or during co-culture with HS27a cells, all indicated on the X axis. Bars show mean +/- SE of 3 independent experiments. All statistically significant comparisons (by unpaired t-test) are as depicted: (i) ROS level, none versus AraC, P = 0.0115, none vs. DNR 0.06, none vs. DEX, P = 0.0035. (ii) % cell death, HS27a AraC vs. DEX, P = 0.0007, HS27a AraC vs. VCR, P = 0.0003.

B. Phallodin/DAPI staining of HS27a MSC exposed alone or exposed to DNR or AraC with or without NAC 5mM.

C. (i) CellROX® ROS assay showing mitochondrial mass (Y axis) of SEM cells in monoculture, baseline set at 1.0 or after coculture with HS27a cells +/-AraC (X axis). Statistically significant comparisons (by unpaired t-test) are as depicted: No HS27a none vs. AraC, P = 0.0115, No HS27a none vs. HS27a none, P = 0.0002, No HS27a AraC vs. HS27a AraC, p = 0.0001. (ii) % apoptosis (annexinV+, DAPI-, Y axis) of SEM cells in monoculture, baseline set at 1.0 or after coculture with HS27a cells +/- AraC (X axis). All statistically significant comparisons (by unpaired t-test) are as depicted: No HS27a none vs. AraC, p = 0.0009, No HS27a AraC vs. HS27a AraC, p = 0.0189. (iii) Cell death (DAPI+, Y axis) of SEM cells in monoculture, baseline set at 1.0 or after coculture with HS27a cells +/- AraC. All statistically significant comparisons (by unpaired t-test) are as depicted: No HS27a none vs. AraC, P = 0.0102, no HS27a AraC vs. HS27a AraC, P = 0.0001.

D. Cell death (DAPI+, Y axis) of SEM cells in monoculture +/- AraC compared with SEM co-cultured in contact with HS27a cells or in a transwell, both with AraC (X axis). All statistically significant comparisons (by unpaired t-test) are as depicted: HS27a AraC vs HS27a transwell AraC, P = 0.0002.

E. (i)ROS levels, (ii) apoptosis and (iii) cell death (Y axis) with no treatment, AraC treatment or AraC treatment + NAC (X axis). Bars show mean +/- SE of 3 independent experiments**.** Significant reductions in ROS (p= 0.002), and apoptosis (p= 0.0479), and a non-significant reduction in cell death ((p = 0.08) by unpaired t-test are shown

Figure 4 AraC and DNR stimulate mitochondrial transfer from healthy donor or HS27a MSC to ALL cells via tunneling nanotubes

A. Phalloidin and DAPI staining of SEM + HD MSC coculture incubated with AraC or VCR at 10X and 40X, as labelled. Red arrows indicate SEM (round cells with prominent nuclei) in physical contact with MSC.

B (i) Mitochondrial transfer by mitotracker® assay (MFI, Y axis), from HS27a to SEM, TOM1 and SD1 ALL cells in contact or in transwell (X axis). All data are mean +/- SE of 3 independent experiments. All statistically significant comparisons (by unpaired t-test) are as depicted: SEM HS27a versus HS27a transwell, P < 0.0001, TOM1 HS27a versus transwell, P < 0.0001, SD1 HS27a versus transwell, P < 0.0001. (ii) Mitochondrial transfer by mitotracker® assay (MFI, Y axis), from healthy donor MSC to healthy donor B-cells (3 independent experiments) or patient ALL cells identified by UKALL14 trial number (UPN) (X axis).

C. Mitochondrial transfer by mitotracker® assay (MFI, Y axis) from HS27a to SEM after co-culture and either no treatment or treatment with AraC, VCR or DEX. All statistically significant comparisons (by unpaired t-test) are as depicted: no treatment vs. AraC, $P < 0.0001$, AraC vs. DEX, $P < 0.0001$, AraC vs. VCR, $P = 0.0003$.

D. (i) Mitochondrial transfer by mitotracker® assay (MFI, Y axis) of SEM cells in co-culture with HS27a MSC after no treatment, AraC treatment or AraC plus NAC 5mM. All statistically significant comparisons (by unpaired t-test) are as depicted: no treatment vs. AraC treatment, $P < 0.0001$, AraC treatment vs AraC plus NAC, $P < 0.0001$. (ii) Mitochondrial mass by mitotracker assay (MFI, Y axis) of SEM cells in co-culture with HS27a MSC after no treatment, DNR treatment or DNR plus NAC 5mM. All statistically significant comparisons (by unpaired t-test) are as depicted: no treatment vs DNR treatment, $P = 0.0002$, DNR treatment vs DNR + NAC, $P = 0.0002$ (iii) Mitochondrial mass by mitotracker assay of REH cells in co-culture with HS27a MSC after no treatment, AraC treatment or AraC plus NAC 5mM. All statistically significant comparisons (by unpaired t-test) are as depicted: no treatment vs AraC treatment, $P < 0.0001$, AraC treatment vs AraC + NAC, $P < 0.0001$.

E. Live cell confocal imaging of HS27a, stained with deep red mitotracker® cells in co-culture with SEM ALL cells stained with DiO. Images were taken at the timepoints indicated (3 minutes apart). The blue and green arrows each indicate the progression of two individual mitochondria along a tunneling nanotube.

F. Agarose gel images showing PCR products from human nuclear and mitochondrial DNA and murine nuclear and mitochondrial DNA, as indicated in each quadrant. Lane 1, MS-5 murine MSC, Lane 2 SEM cells, Lanes 3-5 SEM cells sorted

after co-culture with MS-5, Lanes 6-8 SEM cells sorted after AraC-treated co-culture with MS-5. Human nuclear DNA PCR in lane 5 failed.

Figure 5 Microtubule inhibition blocks mitochondrial transfer and releases ALL cells from ROS-induced, MSC-mediated protection

A. (i) Agarose gel with PCR products from amplification of HS27a mitochondrial DNA, +/- mitochondrial depletion. (ii) Fluorescent microscopy imaging after mitotracker® dye in HS27a +/- mitochondrial depletion. (iii) 40X imaging of mitochondrially-depleted HS27a cells in culture with SEM cells after phalloidin and DAPI staining. (iv) % apoptosis (annexinV+, DAPI-, Y axis) of SEM cells treated with AraC, SEM cells cocultured with HS27a treated with AraC or SEM cocultured with HS27a mito-depleted cells treated with AraC, (X axis). All statistically significant comparisons (by unpaired t-test) are as depicted: HS27a versus Mito-deplete HS27a, P = 0.0008. (v) Percentage cell death (DAPI+, Y axis) of SEM cells treated with AraC, SEM cells cocultured with HS27a treated with AraC, or SEM cocultured with HS27a mito-depleted cells treated with AraC (X axis). All statistically significant comparisons (by unpaired t-test) are as depicted: MH27a versus Mito-deplete HS27a, P = 0.0043. (vi) Percentage cell death or apoptosis (DAPI+ or annexinV+/DAPI- Y axis) of SEM cells + AraC, SEM cells cocultured with HS27a + AraC or SEM cocultured with mito-depleted HS27a + AraC, (X axis). All data are mean +/- SE from 3 independent experiments. All statistically significant comparisons (by unpaired t-test) are as depicted: MH27a versus Mito-deplete HS27a, P < 0.0001.

B. (i) Mitochondrial transfer from HS27a to SEM cells following microtubule damaging blockade. (Mitotracker® MFI, Y axis). Baseline condition is co-culture with no added agents, all other conditions are AraC-treated either alone or with latrunculin-B (lat-B), and nocodazole (nocod) (X axis). All statistically significant comparisons (by unpaired t-test) are as depicted: none versus AraC, P = 0.0005, AraC versus AraC + latrunculin-b, P = 0.0028, AraC vs AraC + nocodazole, P < 0.0001.

C. (i) % viability (Y axis) after treatment of SEM ALL cells with the agents indicated (X axis). (ii) Relative viability (Y axis) after treatment of HS27a cells with the agents indicated (X axis). (iii) % cell death (Y axis) after AraC-treatment of SEM either in monoculture or coculture with HS27a with nil, lat-B nocod, colchicine or VCR added (X axis). All data are mean +/- SE of 3 independent experiments. All statistically significant comparisons (by unpaired t-test) are as depicted: MSC none versus lat-B, P = 0.0004, MSC none versus nocod, P = 0.0018, MSC none versus colchicine, P = 0.0167, MSC none versus VCR, P = 0.0002. (iv) Phalloidin and DAPI staining of HS27a (40X) after exposure to nocodazole or colchicine.

Figure 6 Combining VCR or Dex with AraC or DNR prevents HS27a MSC from developing the characteristic pathology and cytokine secretion patterns of CAF

A. Phalloidin/DAPI staining of AraC or DNR-treated HS27a cells either alone or with VCR or DEX (20X)

B. Cytokines and chemokines (pg/ml, Y axis) secreted by HS27a after AraC or DNR treatment alone or with DEX or VCR. All statistically significant comparisons (by unpaired t-test) are as depicted: IL8 AraC vs AraC + DEX, P = 0.0049, AraC vs AraC

+ VCR, P = 0.0112; IL6 AraC vs AraC + DEX P = 0.0005; CCL2 AraC vs AraC + DEX P = 0.05; IL8 DNR vs DNR + DEX P = 0.0053, DNR vs DNR + VCR P = 0.0364; IL6 DNR vs DNR + DEX, P = 0.0011, DNR vs DNR + VCR P = 0.04.

Figure 7 Cytarabine - but not vincristine or nocodazole - increases ROS and mitochondrial transfer from MSC to ALL cells in a murine xenograft model of ALL and stimulates formation of a nestin+ niche.

A. Live imaging of tumor burden at day -3 and +3 with respect to the treatments given. (i) images with colour scale bar and control mouse are shown. (ii) Quantifcation of the luciferase expression with region of intensity units on the Y axis and experimental conditions on the X axis. P values are 0.0026 for PBS vs AraC, 0.0023 for PBS vs VCR and 0.0098 for PBS vs nocodazole.

B. (i) αSMA staining of MSC isolated and expanded from one control and one AraC - treated mouse (40X) Phalloidin/DAPI staining of MSC isolated and expanded from 3 control, AraC, VCR or nocodazole-treated mice (20X)

C. (i) ROS (MFI, Y axis) and (ii) Mitochondrial mass (green mitotracker® MFI, Y axis) after treatment of mice bearing SEM xenografts with the agents indicated (X axis). Cells were harvested from mice at day +3 after treatment with control, AraC, VCR or nocodazole. All statistically significant comparisons (by unpaired t-test) are as depicted: (i) ROS: PBS vs Ara-C, P = 0.053, (ii) Mitotracker Mass: PBS vs AraC, P = 0.0014.

D. Immunohistochemistry of sections of representative whole femora from AraC and VCR-treated mice. Femora are dual-stained with human CD19 (brown) and murine

nestin (pink). In the AraC example, CD19+ cells are seen closely associating with a nestin+ niche as indicated by the red boxes. In the VCR example, CD19 positive cells (indicated by the brown boxes) are not associated with nestin positive cells (indicated by the pink boxes)

E. (i) Mitochondrial mass (green mitotracker® MFI, Y axis) after treatment of mice bearing SEM xenografts with the agents indicated. SEM cells were harvested from mice treated with PBS, AraC, VCR or AraC+VCR at day +3 after treatment with control, AraC, VCR or AraC + VCR. (ii) Kaplan-Meier survival curves (N=5 mice per group) for mice treated with PBS (blue), AraC (red), VCR (green) and AraC+VCR (purple). All statistically significant comparisons (by unpaired t-test) are as depicted: PBS vs AraC, $P < 0.0001$, AraC vs VCR, $P < 0.0001$. Survival of AraC + VCR-treated mice was significantly greater than each of the other 3 groups by Mantel-Cox test, PBS vs AraC + VCR, $P = 0.0253$, AraC vs AraC + VCR, $P = 0.0080$, VCR vs AraC + VCR 0.0305.

Supplementary figure legends

S1. Schema of in vivo experiments indicating timelines and experimental outputs from two independent experiments

S2. Agarose gel images showing PCR products from DNA extracted from human SEM cells xenografted into NSG mice. Murine nuclear and mitochondrial DNA and human mitochondrial DNA, is present as labelled. Lane 1, murine control bone marrow cells, Lane 2 Human SEM cell control, Lanes 3-6 SEM xenograft

cells sorted on BFP after control treatment Lanes 7-10 SEM xenograft cells sorted on BFP after AraC treatment.

S3. Immunohistochemistry of sections of representative whole femora from each treatment group. Femora are single stained for human CD19 (brown) and murine nestin (pink) plus dual-stained for human CD19 and murine nestin. In the AraC but not the other conditions, CD19+ cells are seen closely associating with a nestin+ niche.

Figure 1 ALL-Cancer associated fibroblasts (ALL-CAF) occur in primary samples from patients with *de novo* ALL undergoing induction chemotherapy.

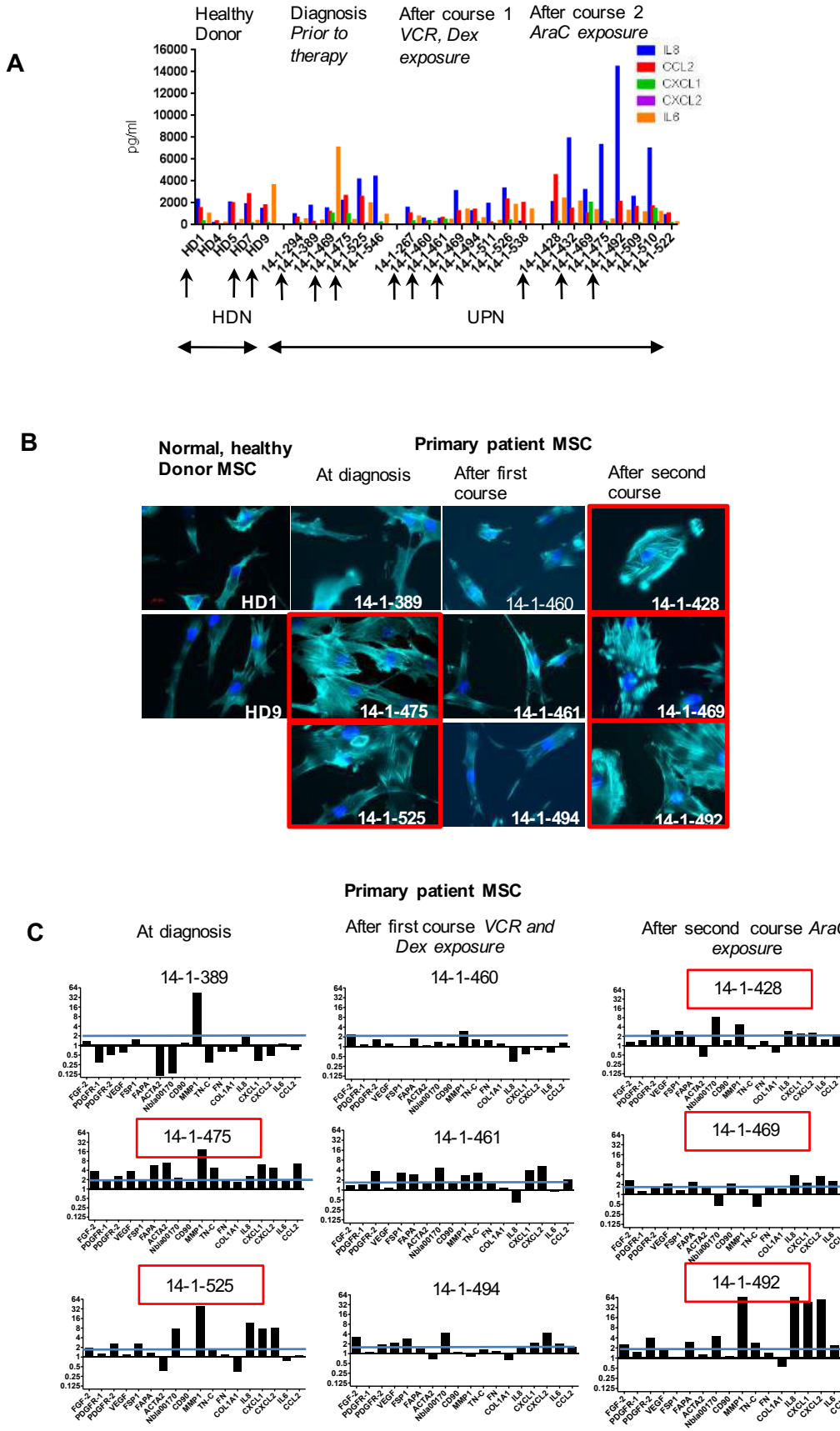

Figure 2 Cytarabine and daunorubicin generate ALL-CAF, *de novo*, from MSCs leading to a diminished B-ALL cell responses to other chemotherapy agents.

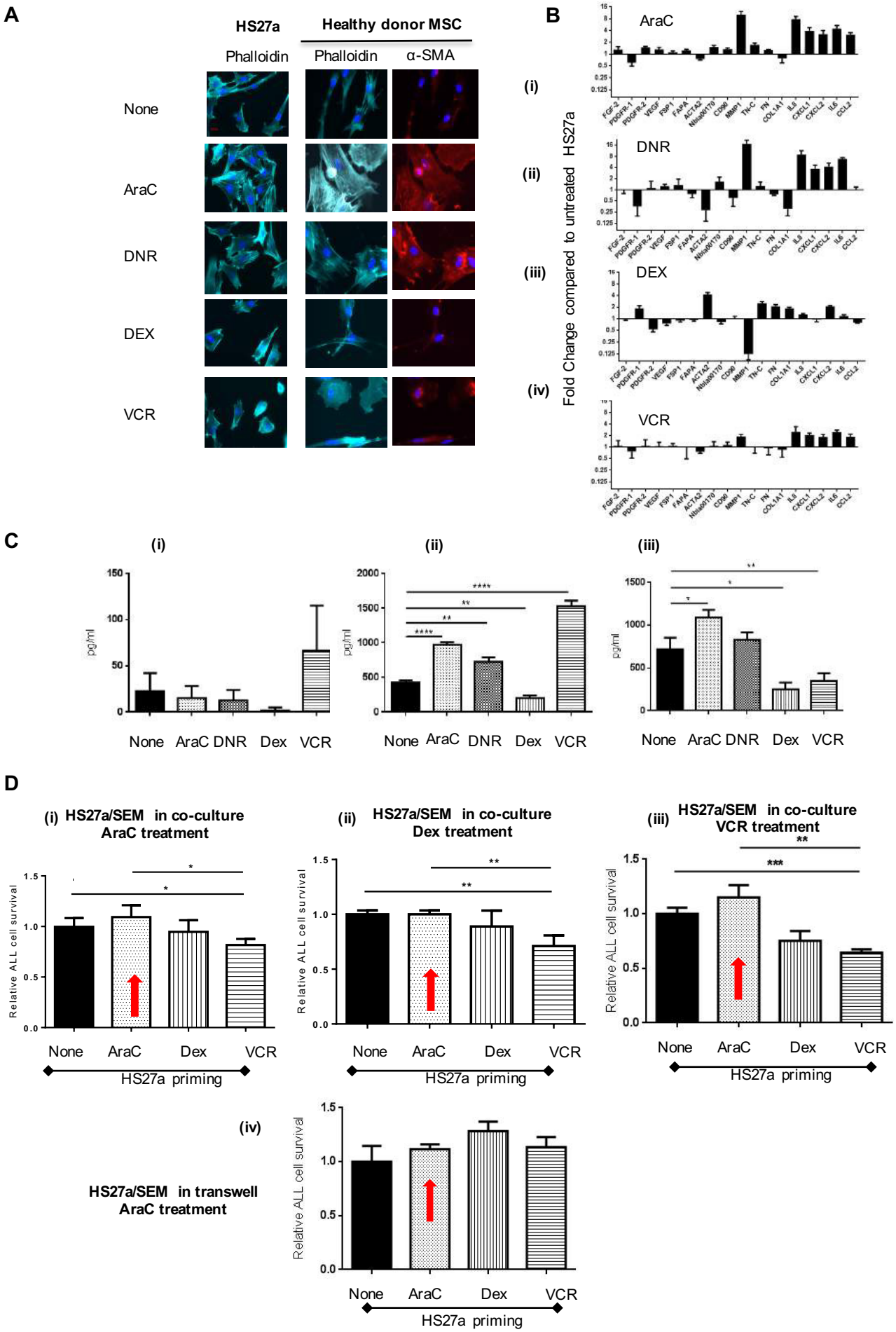

Figure 3

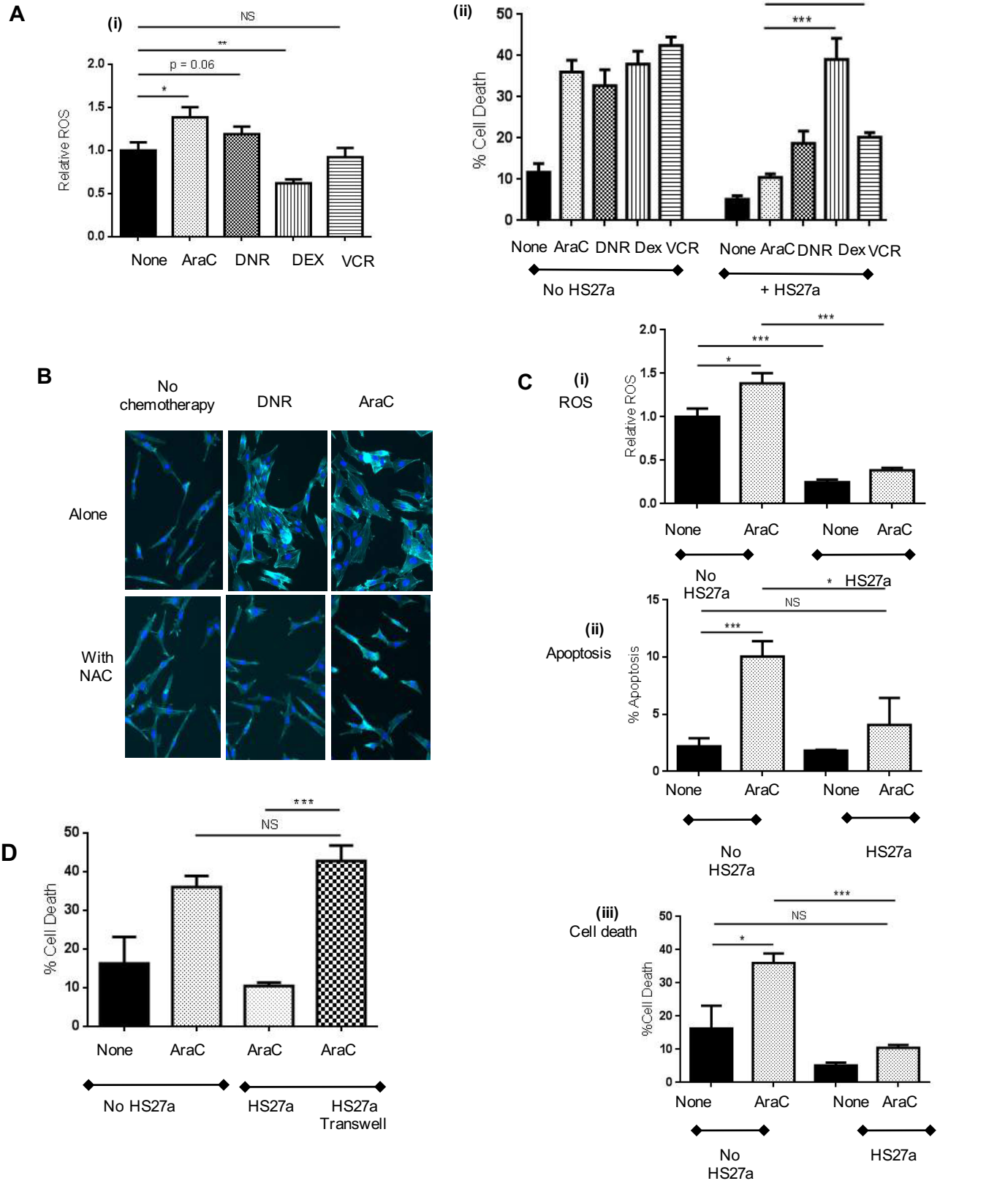
A
(i)
Relative ROS
NS
**
p = 0.06
*
None AraC DNR DEX VCR
(ii)
% Cell Death
***
***
None AraC DNR Dex VCR None AraC DNR Dex VCR
No HS27a
+ HS27a
B
No chemotherapy
DNR
AraC
Alone
With NAC
C
(i)
ROS
Relative ROS
***
***
*
None AraC None AraC
No HS27a
* HS27a
(ii)
Apoptosis
% Apoptosis
NS
***
None AraC None AraC
No HS27a
HS27a
(iii)
Cell death
%Cell Death
***
NS
*
None AraC None AraC
No HS27a
HS27a
D
% Cell Death
***
NS
None AraC AraC AraC
No HS27a
HS27a
HS27a Transwell
E
(i)
ROS
Cell ROX MFI
**
None AraC AraC + NAC
(ii)
Apoptosis
% Apoptosis
*
None AraC AraC + NAC
(iii)
Cell Death
% Cell Death
p = 0.08
None AraC AraC + NAC

Figure 4

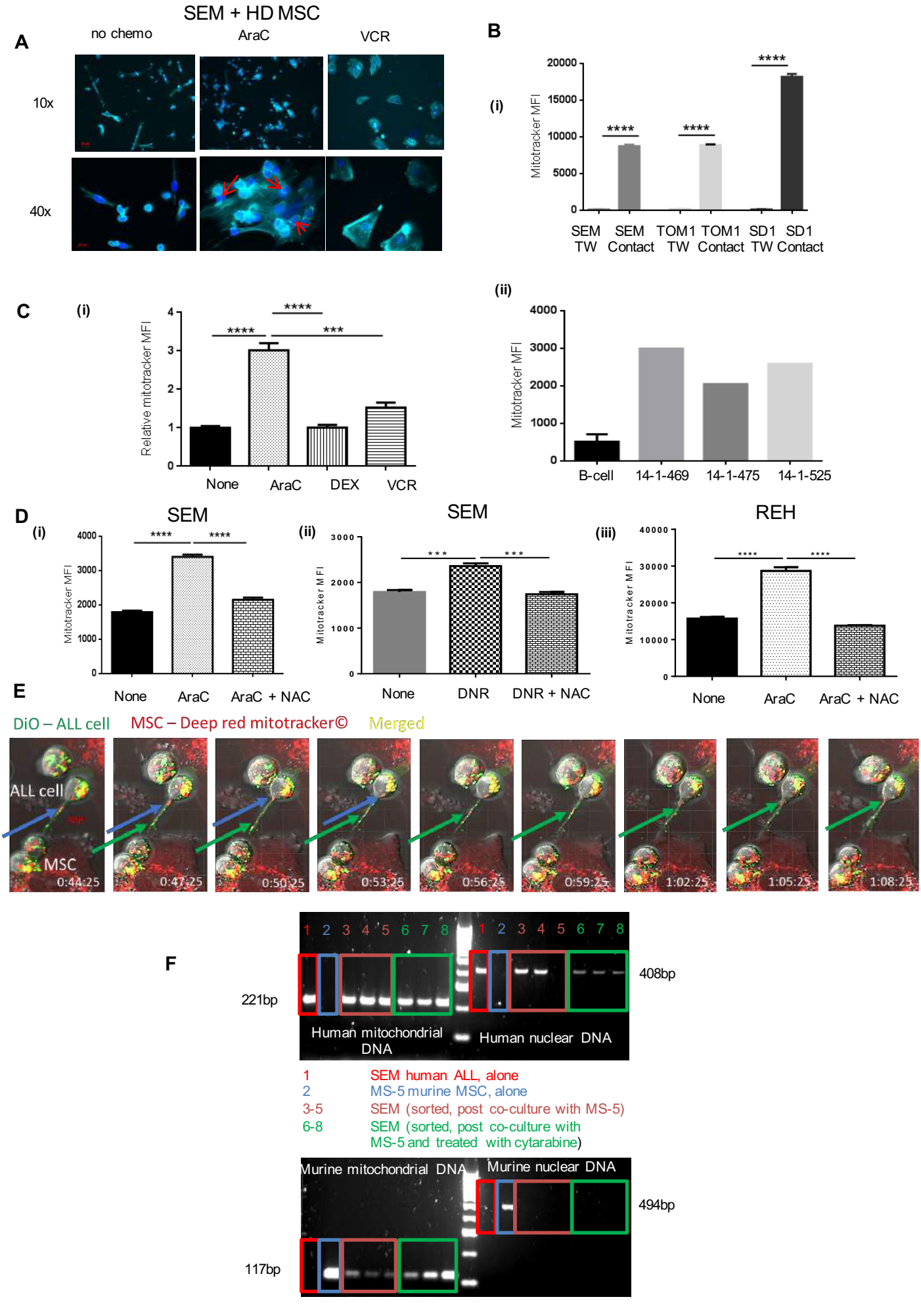
A
SEM + HD MSC
no chemo
AraC
VCR
10x
40x
B
(i)
Mitotracker MFI
20000
15000
10000
5000
0
****
****
****
SEM TW
SEM Contact
TOM1 TW
TOM1 Contact
SD1 TW
SD1 Contact
C
(i)
Relative mitotracker MFI
4
3
2
1
0
****
****
***
None
AraC
DEX
VCR
(ii)
Mitotracker MFI
4000
3000
2000
1000
0
B-cell
14-1-469
14-1-475
14-1-525
D
(i)
SEM
Mitotracker MFI
4000
3000
2000
1000
0
****
****
None
AraC
AraC + NAC
(ii)
SEM
Mitotracker MFI
3000
2000
1000
0
***
***
None
DNR
DNR + NAC
(iii)
REH
Mitotracker MFI
40000
30000
20000
10000
0
****
****
None
AraC
AraC + NAC
E
DiO – ALL cell
MSC – Deep red mitotracker©
Merged
ALL cell
MSC
0:44:25
0:47:25
0:50:25
0:53:25
0:56:25
0:59:25
1:02:25
1:05:25
1:08:25
F
1 2 3 4 5 6 7 8
1 2 3 4 5 6 7 8
221bp
408bp
Human mitochondrial DNA
Human nuclear DNA
1 SEM human ALL, alone
2 MS-5 murine MSC, alone
3-5 SEM (sorted, post co-culture with MS-5)
6-8 SEM (sorted, post co-culture with MS-5 and treated with cytarabine)
Murine mitochondrial DNA
Murine nuclear DNA
117bp
494bp

Figure 5

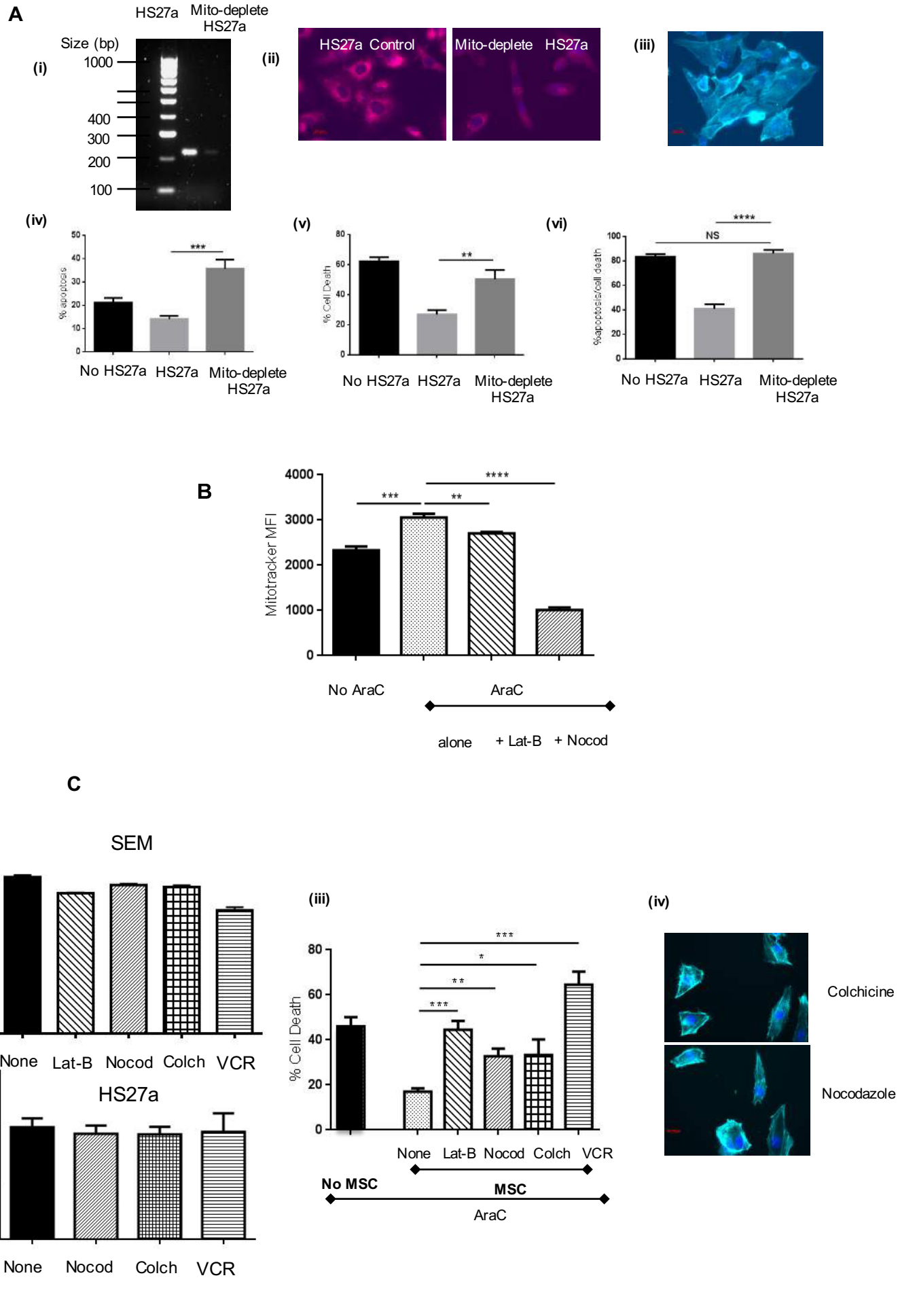
A
HS27a
Mito-deplete HS27a
Size (bp)
(i)
1000
400
300
200
100
(ii)
HS27a Control
Mito-deplete HS27a
(iii)
(iv)
% apoptosis
***
No HS27a
HS27a
Mito-deplete HS27a
(v)
% Cell Death
**
No HS27a
HS27a
Mito-deplete HS27a
(vi)
%apoptosis/cell death
****
NS
No HS27a
HS27a
Mito-deplete HS27a
B
Mitotracker MFI
4000
3000
2000
1000
0
***
**
****
No AraC
AraC
alone
+ Lat-B
+ Nocod
C
(i)
SEM
% ALL cell viability
80
60
40
20
0
None
Lat-B
Nocod
Colch
VCR
(ii)
HS27a
Relative Viability
1.5
1.0
0.5
0.0
None
Nocod
Colch
VCR
(iii)
% Cell Death
80
60
40
20
0
***
*
**
***
None
Lat-B
Nocod
Colch
VCR
No MSC
MSC
AraC
(iv)
Colchicine
Nocodazole

Figure 6

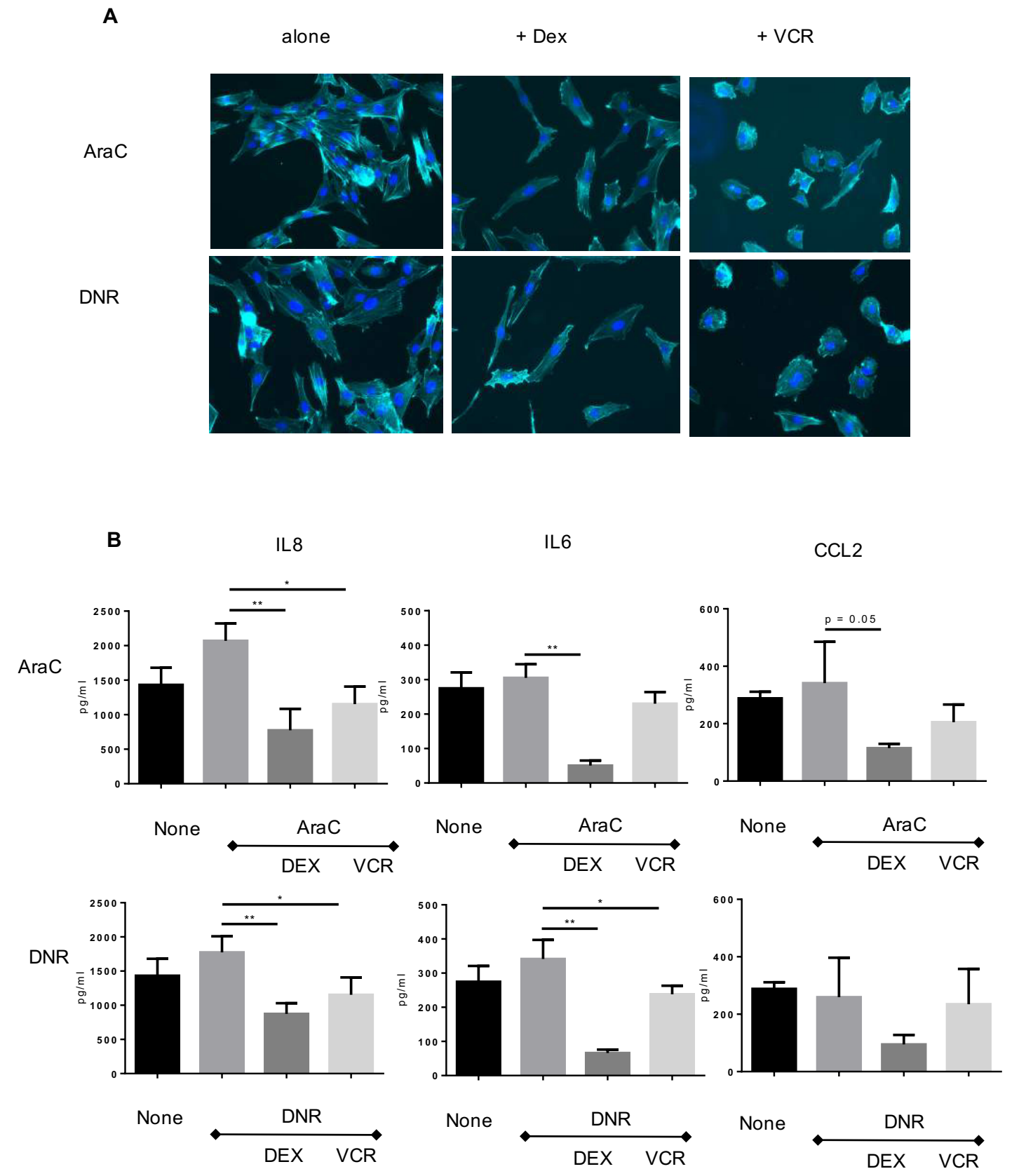
A
alone
+ Dex
+ VCR
AraC
DNR
B
IL8
IL6
CCL2
AraC
DNR
pg/ml
p = 0.05
None
AraC
DNR
DEX
VCR

Figure 7

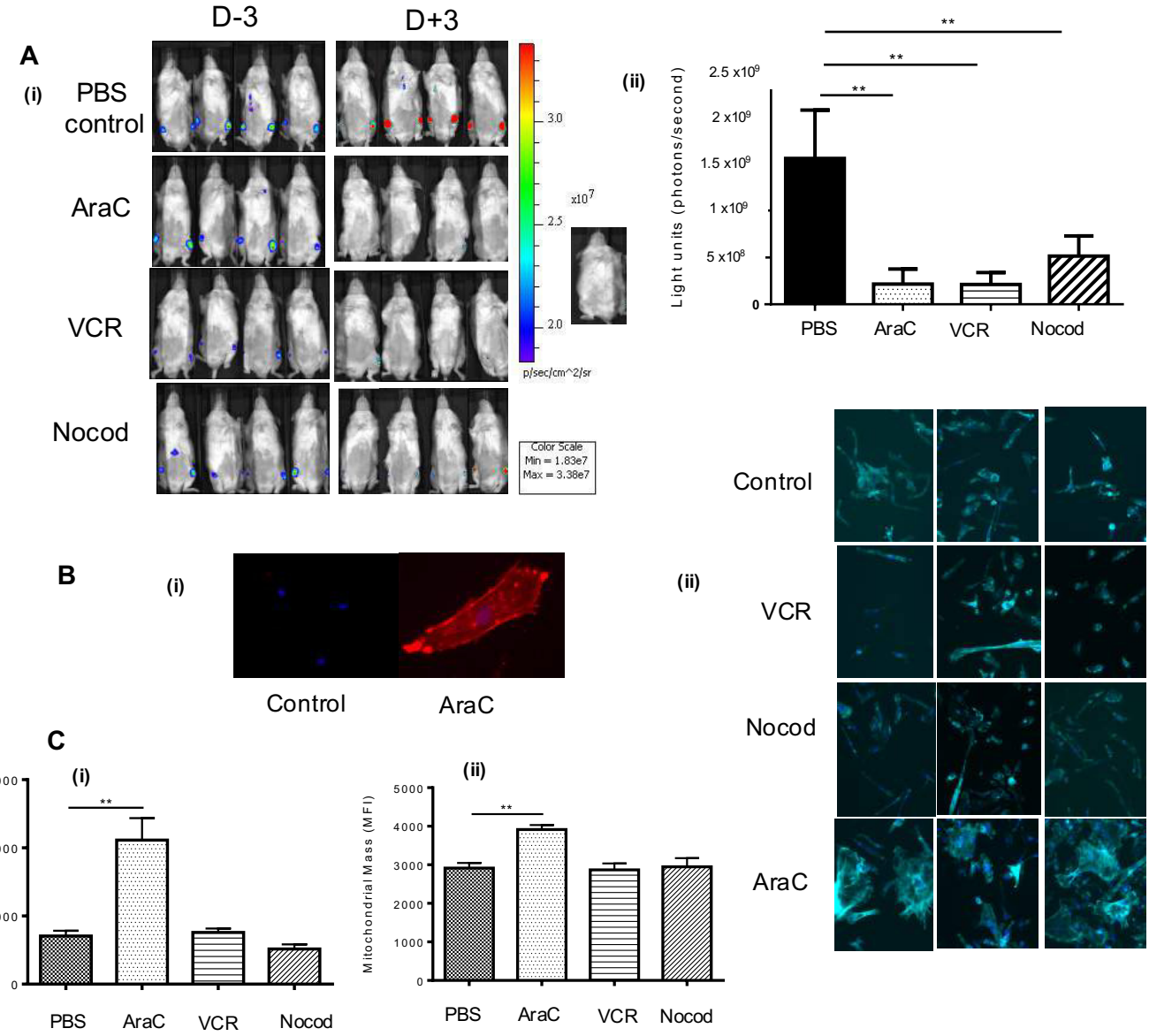
A
(i)
D-3
D+3
PBS control
AraC
VCR
Nocod
x10^7
3.0
2.5
2.0
p/sec/cm^2/sr
Color Scale
Min = 1.83e7
Max = 3.38e7
(ii)
Light units (photons/second)
2.5 x10^9
2 x10^9
1.5 x10^9
1 x10^9
5 x10^8
0
**
PBS
AraC
VCR
Nocod
B
(i)
Control
AraC
(ii)
Control
VCR
Nocod
AraC
C
(i)
Intracellular ROS (MFI)
6000
4000
2000
0
PBS
AraC
VCR
Nocod
(ii)
Mitochondrial Mass (MFI)
5000
4000
3000
2000
1000
0
PBS
AraC
VCR
Nocod
D
(i)
(ii)
E
(i)
Mitotracker MFI
6000
4000
2000
0
****
****
PBS
AraC
VCR
AraC + VCR
(ii)
% survival to humane endpoint
100
50
0
0
10
20
30
Days
PBS
AraC
VCR
AraC + VCR